

# Evidence for multiphase folding of the central Indian Ocean lithosphere

K.S. Krishna National Institute of Oceanography, Dona Paula, Goa 403004, India

J.M. Bull School of Ocean and Earth Science, Southampton Oceanography Centre, Southampton University, Southampton SO14 3ZH, UK

R.A. Scrutton Department of Geology and Geophysics, Edinburgh University, Edinburgh EH9 3JW, UK

## ABSTRACT

Long-wavelength (100–300 km) folding in the central Indian Ocean associated with the diffuse plate boundary separating the Indian, Australian, and Capricorn plates is Earth's most convincing example of organized large-scale lithospheric deformation. To test the timing and mechanics of this deformation as implied by plate-kinematic and deformation models, we present a new analysis of the seismic stratigraphy of the Bengal Fan sediments. This analysis shows that the folding of the oceanic lithosphere was multiphase, with major events occurring in the Miocene (8.0–7.5 Ma), Pliocene (5.0–4.0 Ma), and Pleistocene (0.8 Ma). The Miocene phase was the most intense and involved deformation of an area south of 1°S, whereas in the Pliocene the activity shifted northward. In the final phase (Pleistocene), the activity was focused in the equatorial region. No evidence was found for deformation prior to 8.0–7.5 Ma. The spatial extent of the Pleistocene folding event overlaps the Pliocene and/or Miocene folding events and coincides with both the area of most active faulting and the zone of greatest historical seismicity. The seismic data show that the timing of reverse faulting, and thus more significant shortening of the lithosphere, generally coincided with the phases of folding, but there are examples of folding of the oceanic lithosphere without associated reverse faulting.

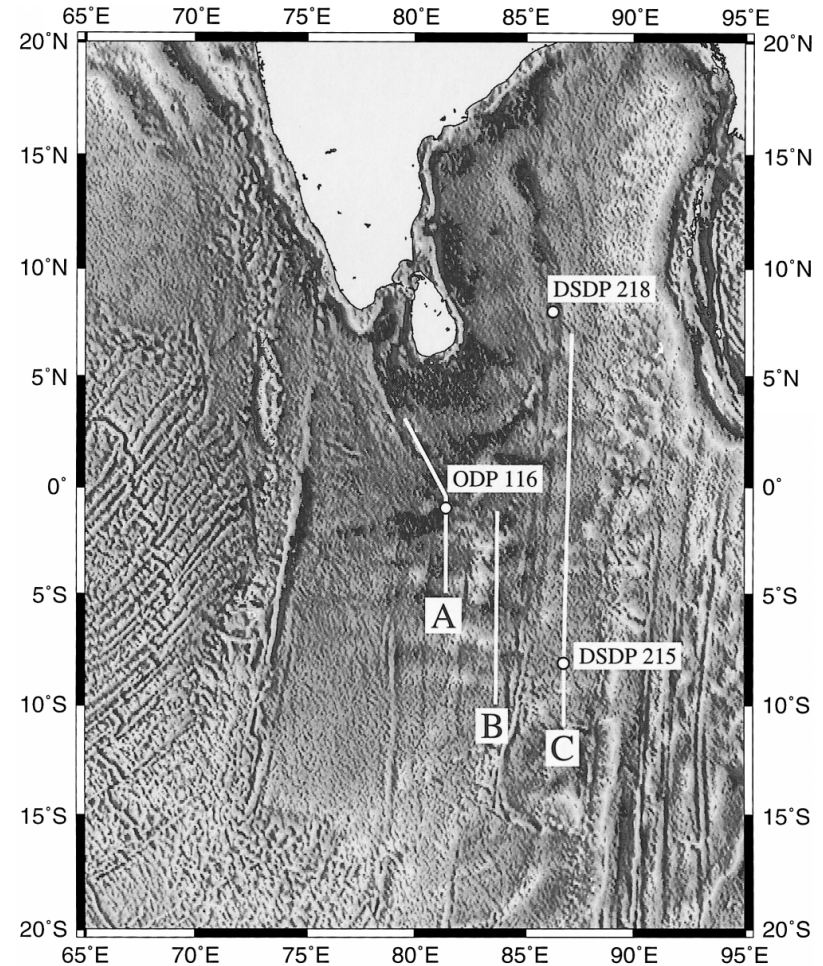


Figure 1. Locations of the three long seismic reflection profiles in central Indian Ocean superimposed on satellite gravity field (Sandwell and Smith, 1997). Seismic stratigraphic interpretation of profiles A, B, and C are shown as line drawings in Figure 2. Circles indicate locations of DSDP Sites 215 and 218 and ODP Leg 116 sites.

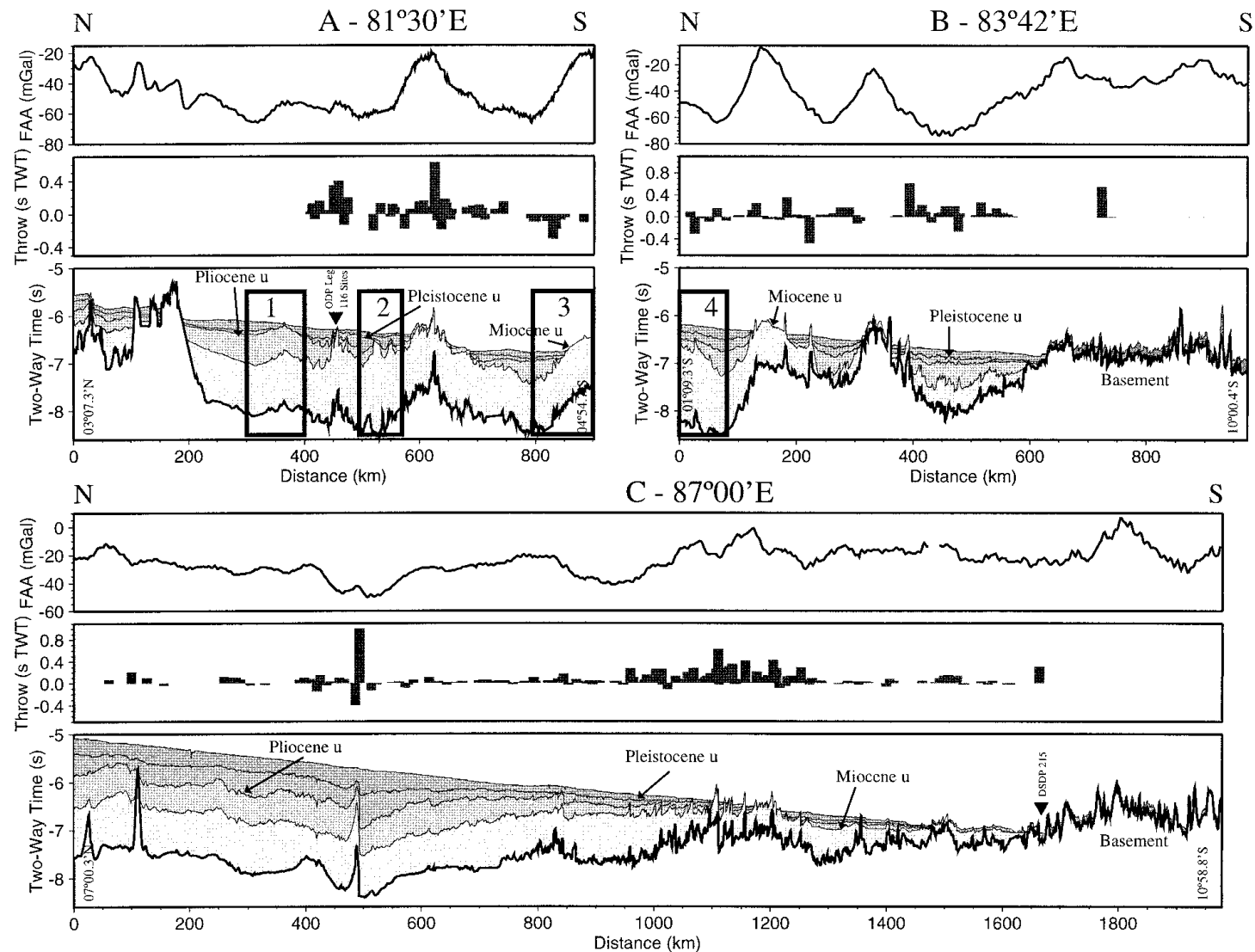
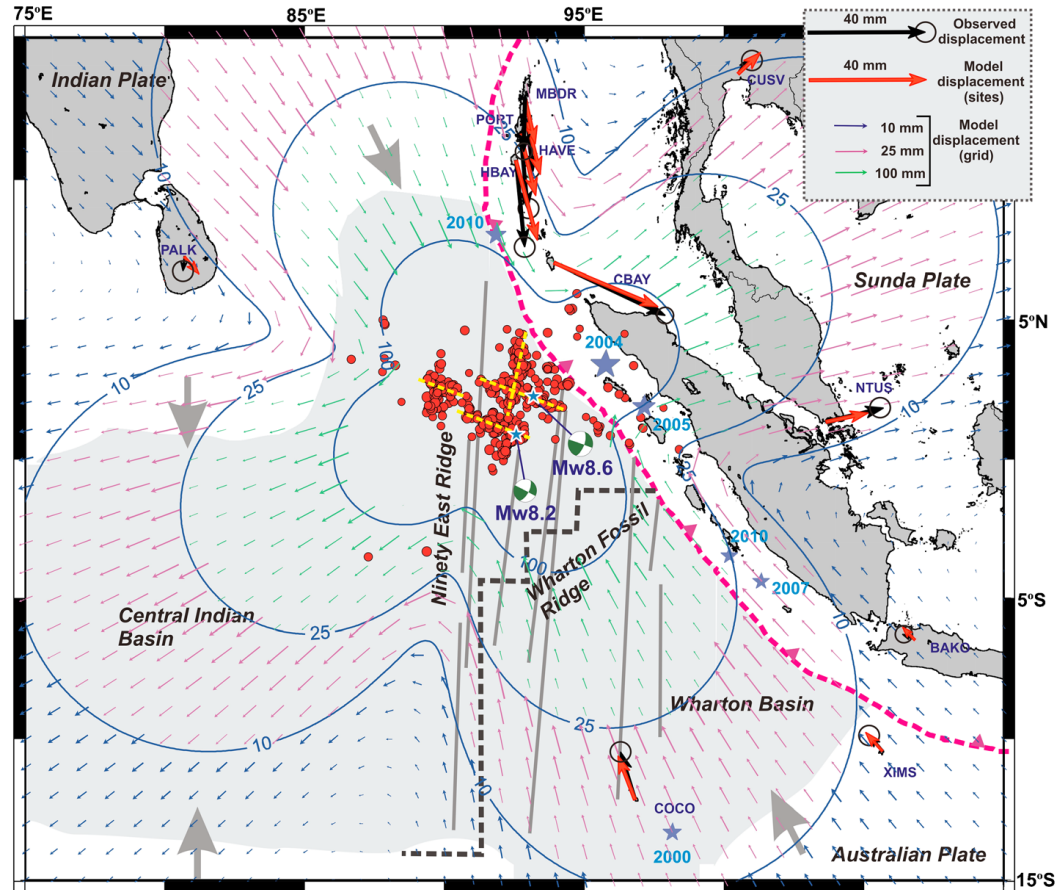
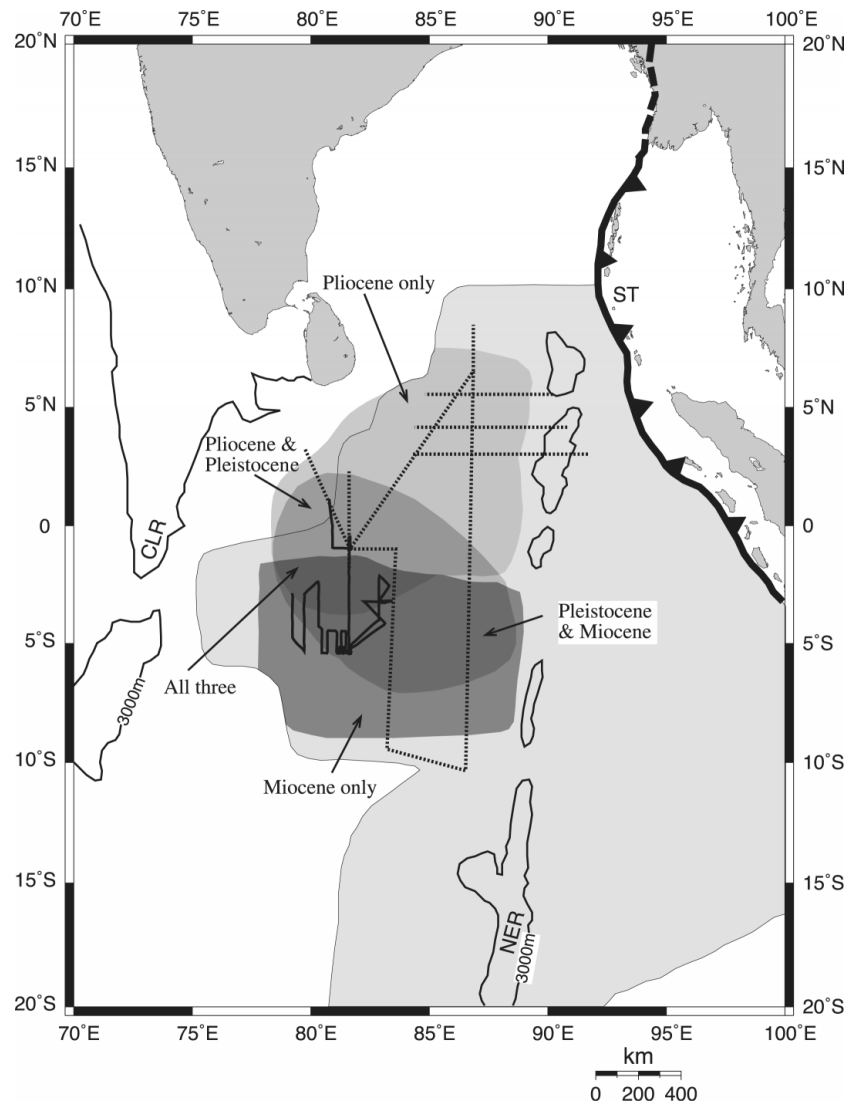


Figure 2. Line drawings of interpreted seismic data along profiles A (81.5°E), B (83.7°E), and C (87.0°E). Panels outlined and numbered 1, 2, 3, and 4 are in Figure 3 and show how unconformities have recorded formation of long-wavelength folding at different times. Panel 1 shows clear Pliocene and Pleistocene folding; panel 2 shows Miocene and Pliocene folding; panel 3 shows only Miocene folding; panel 4 shows Miocene and Pleistocene folding. Some steep, isolated basement rises north of 200 km along profile A act as barrier limiting western extent of Bengal Fan sediments. Southern extent of Bengal Fan sediments is seen on both profiles B and C at about same latitude, 7°40'S. Major basement undulation covered with thin upper Miocene sediments is observed along profile B. This was initially part of basement structure of Afanasy Nikitin Seamount, but during late Miocene time, it was uplifted to form part of a long-wavelength fold structure. Positions of reverse faults and their vertical throws are shown above each profile. Free-air gravity anomalies (FAA) for each profile show presence of 100–300-km-wavelength folding.

YADAV ET AL.:  $M_w$  8.6 2012 INDIAN OCEAN EARTHQUAKE



**Figure 1.** The 11 April 2012 earthquakes and coseismic offsets derived from GPS measurements at various IGS sites and at permanent GPS sites in the Andaman-Nicobar region (shown with black arrows with error bars). The bold gray arrows represent the compressional regime of the diffused plate boundary region (shaded with light gray color) between the Indian and Australian plates [Gordon *et al.*, 1998]. The yellow dashed lines denote the rupture planes of the 11 April 2012 earthquakes [Yue *et al.*, 2012]. Arrows with different colors show the simulated coseismic offsets due to the slip models by Yue *et al.* [2012] using the layered spherical earth [Pollitz, 1997]. The purple stars are other earthquakes discussed in the text. The north-south gray lines indicate the fracture planes in the Wharton and Central Indian basin.

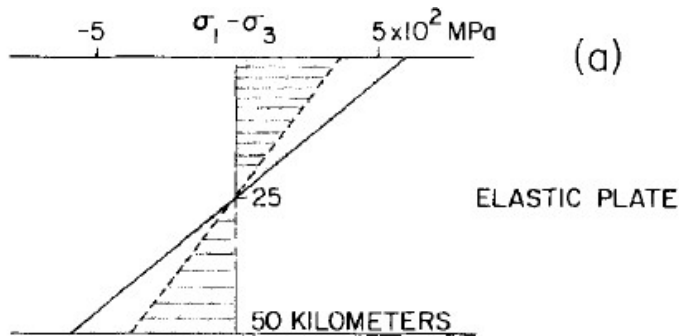


**Figure 4. Deformation of oceanic lithosphere in space and time in central Indian Ocean. Shading shows position of diffuse plate boundary separating Capricorn, Indian, and Australian plates (Royer and Gordon, 1997). Superimposed on this area are approximate spatial extents of long-wavelength folding at three different times (8.0–7.5, 5.0–4.0, 0.8 Ma). Note that earliest folding event is concentrated in south, whereas Pliocene event (5.0–4.0 Ma) extends farther northward. Spatial distribution of Pleistocene folding event overlaps Pliocene and/or Miocene folding event zones and coincides with area of most active faulting and zone of greatest historical seismicity. Positions of seismic reflection profiles: solid lines from Bull and Scrutton (1992); dotted lines from Krishna et al. (1998). NER—Ninetyeast Ridge, CLR—Chagos-Laccadive Ridge system, and ST—Sumatran Trench.**

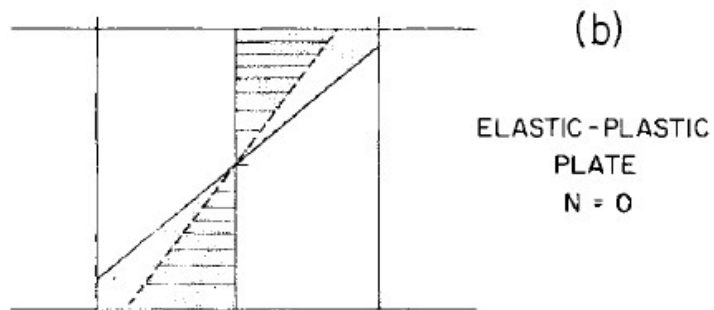
**Notes on BB**

**buckling problem**

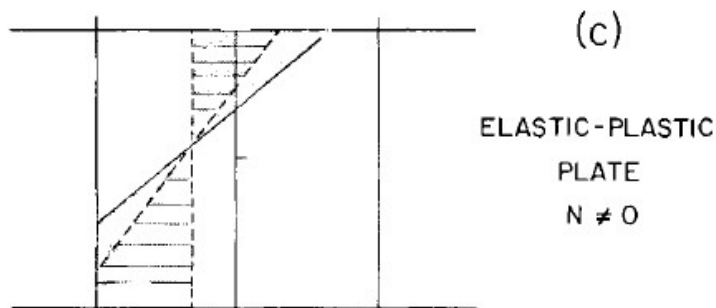
# finite yield strength



Stress difference are linearly proportional to distance from the neutral axis in the elastic plate.



Real earth materials do have a finite strength.



The plate behaves elastically up to the yield stress, at which point the plate fails. Additional strain causes no increases in stress.

# finite yield strength

Three zones of rock behavior:

## 1. Brittle zone

Upper cool lithosphere. Governed by brittle failure. Strength increases with overburden pressure but is insensitive to temperature, strain rate and rock type.

## 2. Semi-brittle zone

Both brittle and ductile processes occur, usually not included in the yield envelope.

## 3. Ductile zone

Lower hot lithosphere. Governed by ductile flow. Strength is insensitive to pressure effects but decreases with decreasing strain rate.

## Friction of Rocks

By J. BYERLEE

Abstract - Experimental results in the published literature show that at low normal stress the shear stress required to slide one rock over another varies widely between experiments. This is because at low stress rock friction is strongly dependent on surface roughness. At high normal stress that effect is diminished and the friction is nearly independent of rock type. If the sliding surfaces are separated by gouge composed of montmorillonite or vermiculite the friction can be very low.

Key words: Rock mechanics; Friction; Faulting surfaces.

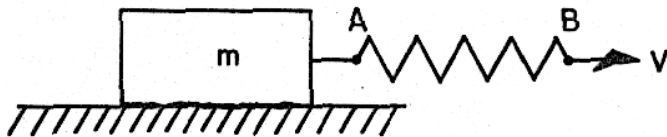


Figure 1  
Schematic diagram of a typical friction experiment. For explanation see text.

U.S. Geological Survey, Menlo Park, California 94025, USA.

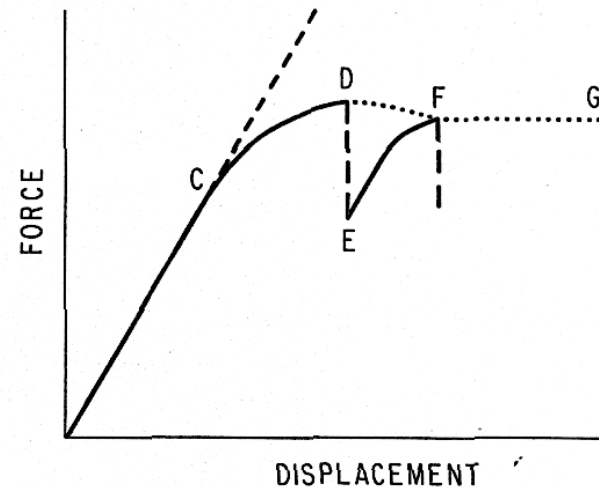


Figure 2  
Schematic diagram of the frictional force plotted as a function of displacement of the rider. See text for explanations.

# MAXIMUM FRICTION

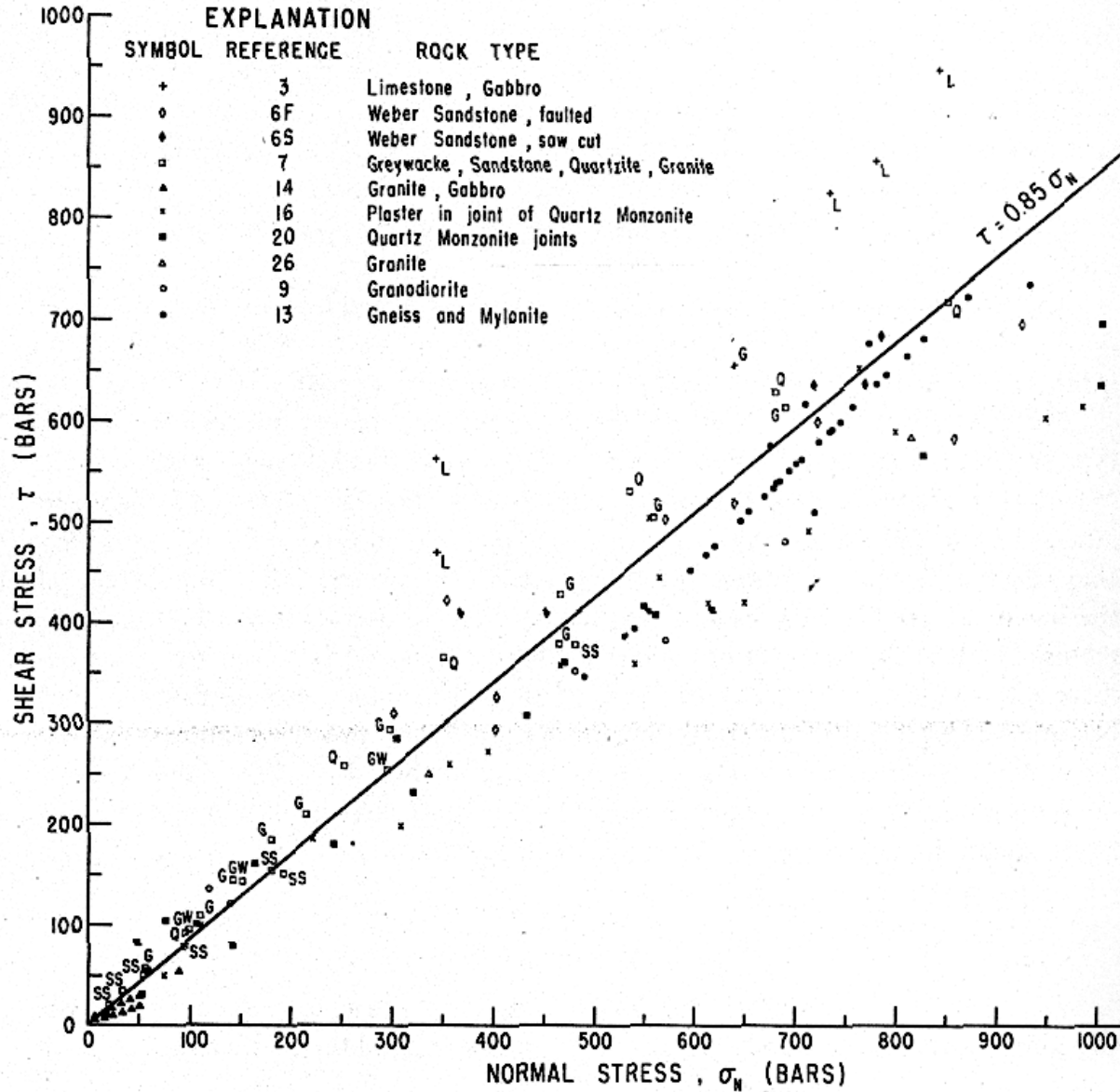


Figure 5  
 Shear stress plotted as a function of normal stress at the maximum friction for a variety of rock types at normal stresses to 1000 bars.

Notes on BB

YSE overview

ductile deformation

## Limits on Lithospheric Stress Imposed by Laboratory Experiments

W. F. BRACE

*Department of Earth and Planetary Sciences, Massachusetts Institute of Technology, Cambridge, Massachusetts 02139*

D. L. KOHLSTEDT

*Department of Materials Science and Engineering, Cornell University, Ithaca, New York 14853*

Laboratory measurements of rock strength provide limiting values of lithospheric stress, provided that one effective principal stress is known. Fracture strengths are too variable to be useful; however, rocks at shallow depth are probably fractured so that frictional strength may apply. A single linear friction law, termed Byerlee's law, holds for all materials except clays, to pressures of more than 1 GPa, to temperatures of 500°C, and over a wide range of strain rates. Byerlee's law, converted to maximum or minimum stress, is a good upper or lower bound to observed in situ stresses to 5 km, for pore pressure hydrostatic or subhydrostatic. Byerlee's law combined with the quartz or olivine flow law provides a maximum stress profile to about 25 or 50 km, respectively. For a temperature gradient of 15°K/km, stress will be close to zero at the surface and at 25 km (quartz) or 50 km (olivine) and reaches a maximum of 600 MPa (quartz) or 1100 MPa (olivine) for hydrostatic pore pressure. Some new permeability studies of crystalline rocks suggest that pore pressure will be low in the absence of a thick argillaceous cover.

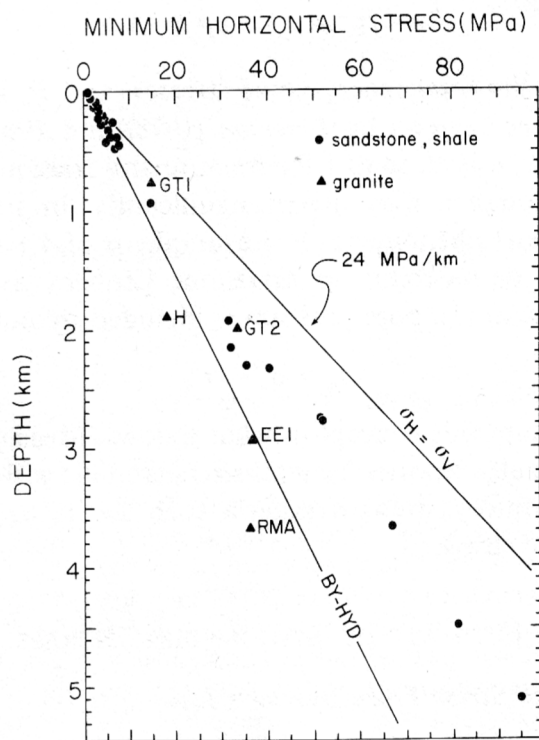


Fig. 2. The minimum total horizontal stress measured in the United States. Symbols as in Figure 1 [McGarr and Gay, 1978].

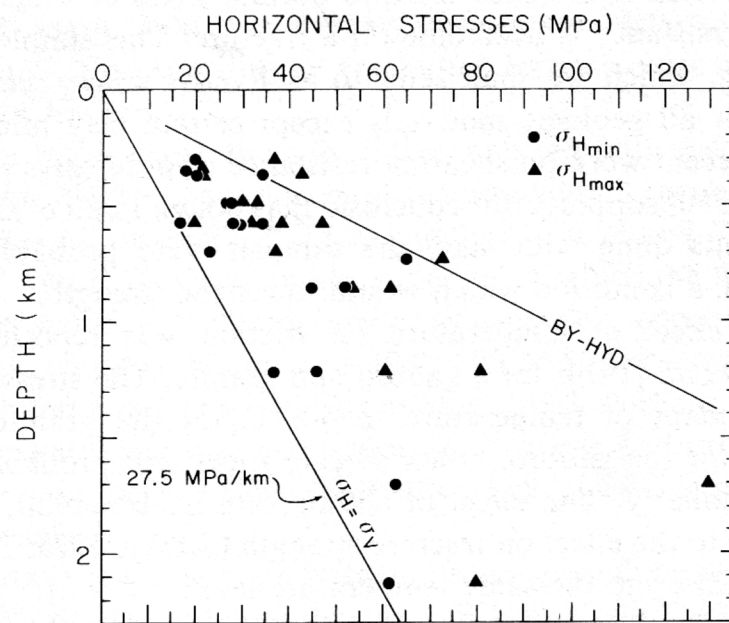


Fig. 3. Total horizontal stresses measured in Canada [McGarr and Gay, 1978]. Symbols as in Figure 1.

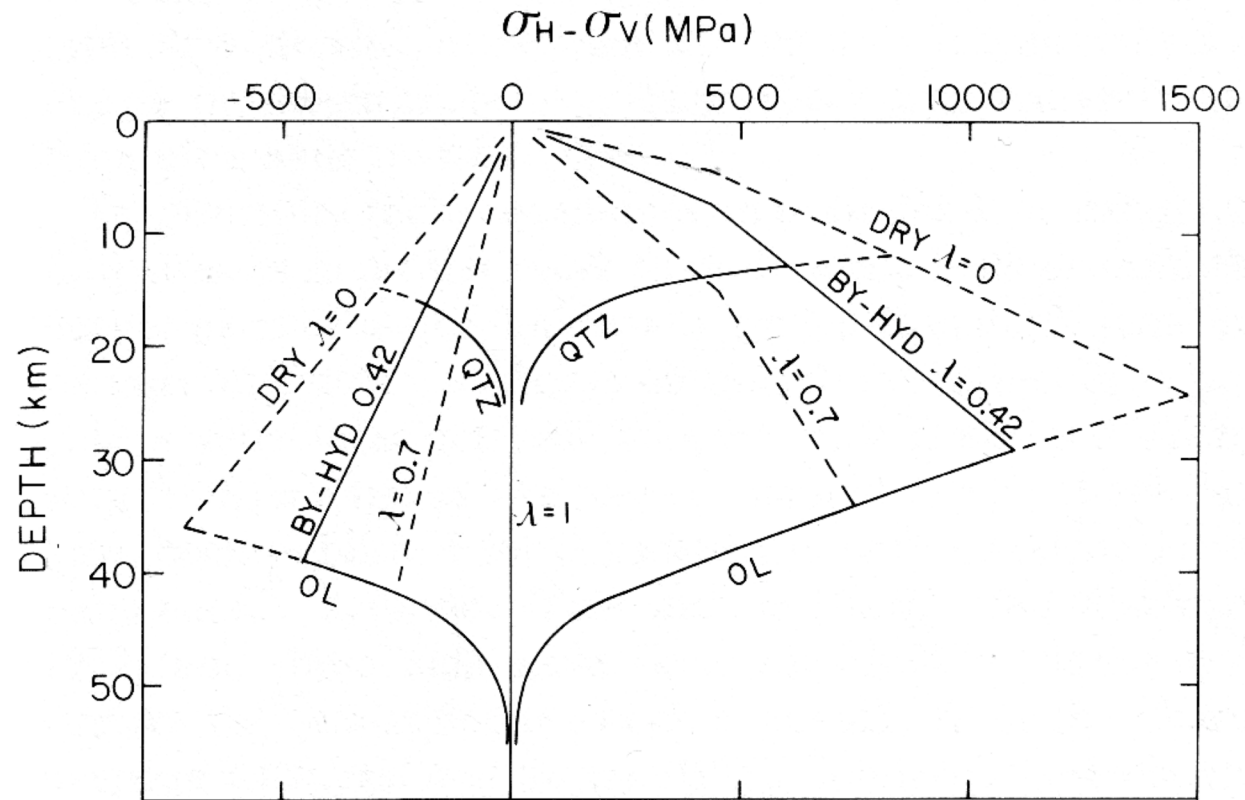


Fig. 5. Difference between maximum or minimum horizontal stress and the vertical stress as a function of depth. Values of  $\lambda$  give pore pressure level. See also Figure 4.

# Rheology of the Lower Crust and Upper Mantle: Evidence from Rock Mechanics, Geodesy, and Field Observations

Roland Bürgmann<sup>1</sup> and Georg Dresen<sup>2</sup>

<sup>1</sup>Department of Earth and Planetary Science, University of California, Berkeley, California 94720; email: burgmann@seismo.berkeley.edu

<sup>2</sup>GeoForschungsZentrum Potsdam, D-14473 Potsdam, Germany; email: dre@gfz-potsdam.de

## Key Words

brittle-ductile transition, deformation mechanisms, postseismic relaxation, shear zones, viscosity

## Abstract

Rock-mechanics experiments, geodetic observations of postloading strain transients, and micro- and macrostructural studies of exhumed ductile shear zones provide complementary views of the style and rheology of deformation deep in Earth's crust and upper mantle. Overall, results obtained in small-scale laboratory experiments provide robust constraints on deformation mechanisms and viscosities at the natural laboratory conditions. Geodetic inferences of the viscous strength of the upper mantle are consistent with flow of mantle rocks at temperatures and water contents determined from surface heat-flow, seismic, and mantle xenolith studies. Laboratory results show that deformation mechanisms and rheology strongly vary as a function of stress, grain size, and fluids. Field studies reveal a strong tendency for deformation in the lower crust and uppermost mantle in and adjacent to fault zones to localize into systems of discrete shear zones with strongly reduced grain size and strength. Deformation mechanisms and rheology may vary over short spatial (shear zone) and temporal (earthquake cycle) scales.

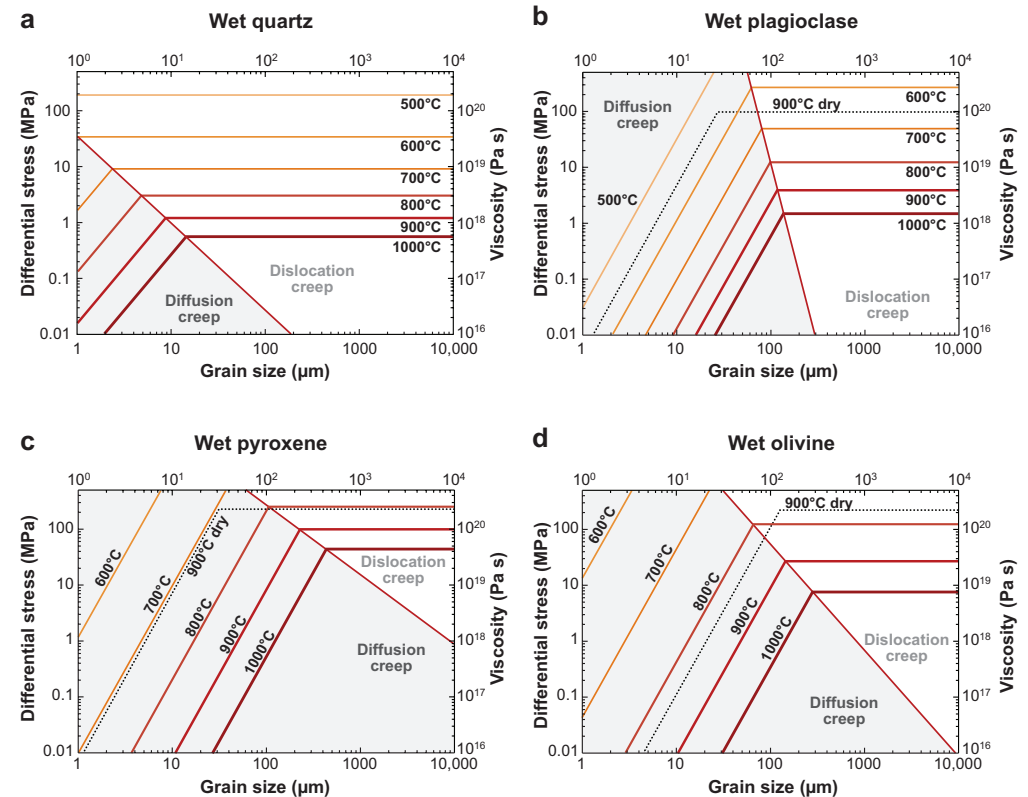
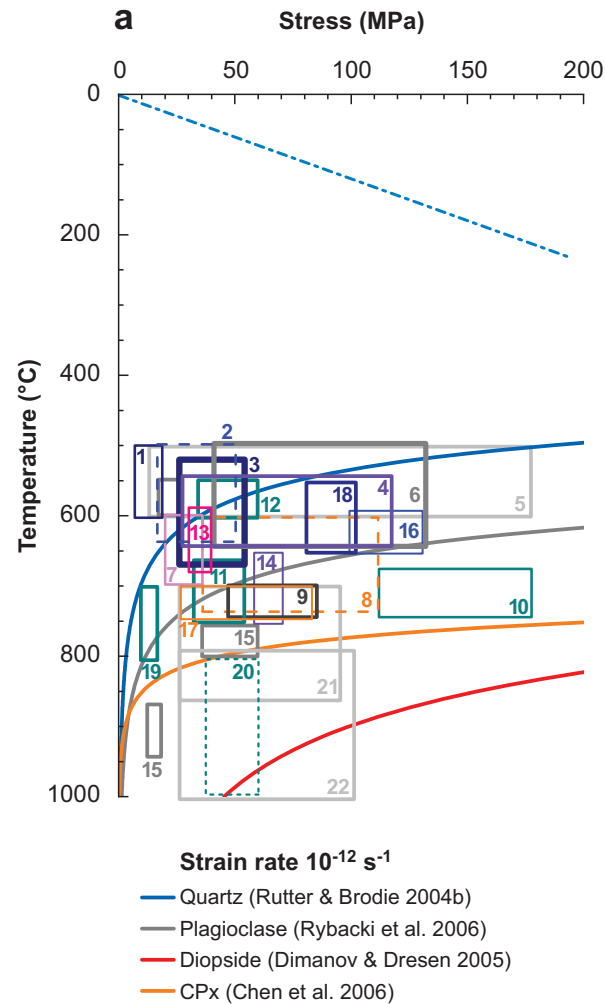


**Figure 3**

Deformation mechanism maps for wet (nominally saturated in water) rheologies of (a) quartz (Rutter & Brodie 2004a,b), (b) feldspar (Rybacki et al. 2006), (c) pyroxene [wet (Dimanov & Dresen 2005), dry (Bystricky & Mackwell 2001)] and (d) olivine (Hirth & Kohlstedt 2003). For construction of the maps, a strain rate of  $10^{-12} \text{ s}^{-1}$ , a geotherm corresponding to a heat flow of  $80 \text{ mW m}^{-2}$ , and a rock density of  $2.8 \text{ g cm}^{-3}$  were assumed. For these conditions, diffusion-controlled creep dominates in rocks with a grain size smaller than  $\sim 200 \mu\text{m}$  at temperatures of approximately  $500^\circ\text{C}$  to  $900^\circ\text{C}$  except for quartz. For comparison, a dotted line shows the anhydrous relationship at  $900^\circ\text{C}$ . Viscosity estimates from geodetic measurements between  $1 \times 10^{18}$  and  $10 \times 10^{19} \text{ Pa s}$  are in good agreement with the rheology of rocks containing at least trace amounts of  $\text{H}_2\text{O}$ , but not with dry rocks.

## lower crust



## upper mantle

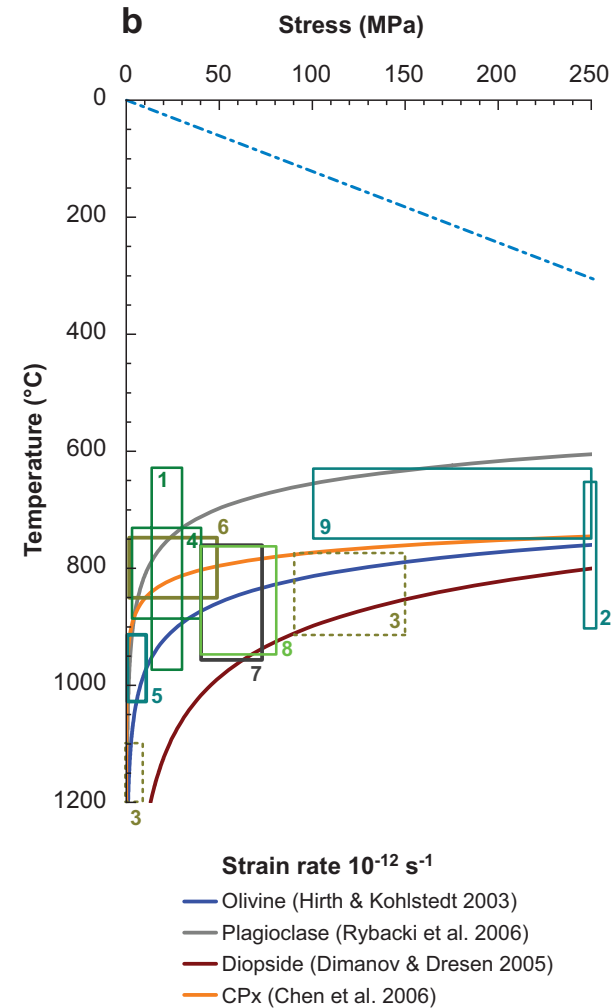


**Figure 7**

Paleostress estimates from mylonite shear zones transecting lower crust (*a*) and upper mantle (*b*). Each box represents stress-temperature estimates for a particular shear zone. A list with all numbered references is provided in the **Supplemental Appendix**. Stress estimates are mostly based on the inverse relation between recrystallized grain size and flow stress (Twiss 1977, van der Wal et al. 1993). Graphs indicate extrapolated laboratory data for the dislocation creep of rocks at hydrous conditions. The field data from lower-crustal shear zones are bracketed by the flow strength of quartzite and pyroxenite. Paleostress estimates from upper-mantle shear zones are bracketed by the flow strength of anorthosite and pyroxenite. The field estimates cluster between approximately 10 and 50 MPa in lower-crustal and upper-mantle shear zones. However, paleostresses could be severely overestimated if deformation in shear zones is dominated by diffusion-controlled creep.

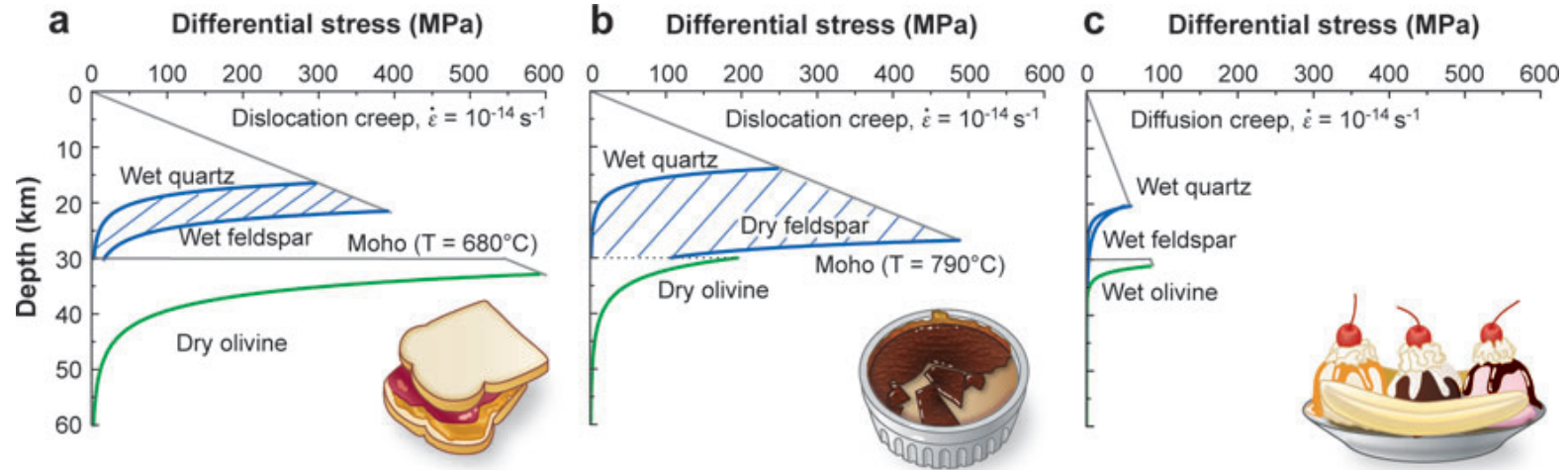


**Figure 1**

Schematic view of alternative first-order models of strength through continental lithosphere. In the upper crust, frictional strength increases with pressure and depth. In the two left panels a coefficient of friction following Byerlee's law and hydrostatic fluid pressure (ratio of pore pressure to lithostatic pressure  $\lambda = 0.4$ ) are assumed in a strike-slip tectonic regime. In the right panel, low friction due to high pore fluid pressure ( $\lambda = 0.9$ ) is assumed. (a) A jelly sandwich strength envelope is characterized by a weak mid-to-lower crust and a strong mantle composed dominantly of dry olivine (Hirth & Kohlstedt 2003). (b) The crème brûlée model posits that the mantle is weak (in the case shown resulting from a higher geotherm, adding water would produce a dramatic further strength reduction). The dry and brittle crust defines the strength of the lithosphere. (c) The banana split model considers the weakness of major crustal fault zones throughout the thickness of the lithosphere, caused by various strain weakening and feedback processes. Owing to small grain size in shear zones, deformation in the lower crust and upper mantle is assumed to be accommodated by linear diffusion creep (grain size of  $50 \mu\text{m}$ ). Strength envelopes are based on flow law parameters presented in **Supplemental Table 1**. For the crust, a quartz and feldspar rheology was used (Rutter & Brodie 2004a,b; Rybacki et al. 2006). We assumed a geothermal gradient corresponding to surface heat flow of  $80 \text{ mW m}^{-2}$  ( $90 \text{ mW m}^{-2}$  for the crème brûlée model to avoid overly strong, dry lower crust) and a uniform strain rate of  $10^{-14} \text{ s}^{-1}$ .

[▶ Supplemental Material](#)

# The long-term strength of continental lithosphere: “jelly sandwich” or “crème brûlée”?

**E.B. Burov**, *Laboratoire de Tectonique, University of Paris 6, 4 Place Jussieu, 75252 Paris Cedex 05, France, evgenii.burov@lgs.jussieu.fr*, and **A.B. Watts**, *Department of Earth Sciences, University of Oxford, Parks Road, Oxford OX1 3PR, UK, tony.watts@earth.ox.ac.uk*

---

## ABSTRACT

There has been much debate recently concerning the long-term (i.e., >1 m.y.) strength of continental lithosphere. In one model, dubbed jelly sandwich, the strength resides in the crust and mantle, while in another, dubbed crème brûlée, the mantle is weak and the strength is limited to the crust. The different models have arisen because of conflicting results from elastic thickness and earthquake data. We address the problem here by first reviewing elastic thickness estimates and their relationship to the seismogenic layer thickness. We then explore, by numerical thermomechanical modeling, the implications of a weak and strong mantle for structural styles. We argue that, irrespective of the actual crustal strength, the crème-brûlée model is unable to explain either the persistence of mountain ranges or the integrity of the downgoing slab in collisional systems. We conclude that while the crème-brûlée model may apply in some tectonic settings, a more widely applicable model is the jelly sandwich.

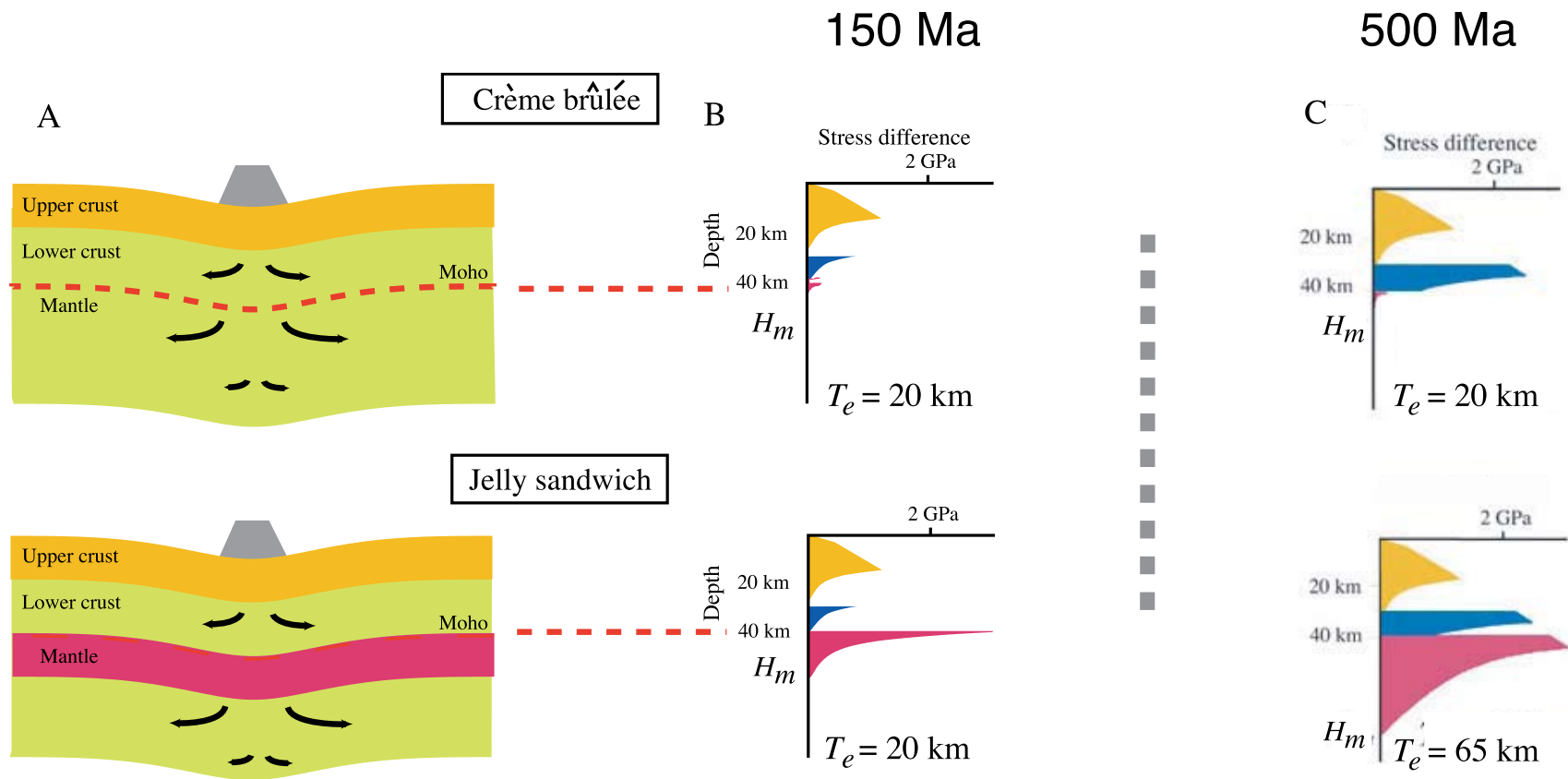


Figure 1. Schematic diagram illustrating different models for the long-term strength of continental lithosphere. In the crème-brûlée model, the strength is confined to the uppermost brittle layer of the crust, and compensation is achieved mainly by flow in the weak upper mantle. In the jelly sandwich model, the mantle is strong and the compensation for surface loads occurs mainly in the underlying asthenosphere. (A) Models of deformation. Arrows schematically show the velocity field of the flow. (B) Brace-Goetze failure envelopes for a thermotectonic age of 150 Ma, a weak, undried granulite lower crust, a uniform strain rate of  $10^{-15} \text{ s}^{-1}$ , and either a dry (jelly sandwich) or wet (crème brûlée) olivine mantle.  $H_m$  is the short-term mechanical thickness of the lithosphere;  $T_e$  is the long-term elastic thickness. Other parameters are as given in Tables 1 and 2. The two envelopes match those in Figures 5B and 5D of Jackson (2002). They yield a  $T_e$  of 20 km (e.g., Burov and Diament, 1995), which is similar to the thickness of the most competent layer. This is because the competent layers are mechanically decoupled by weak ductile layers and so the inclusion of a weak lower crust or strong mantle contributes little to  $T_e$ . (C) Brace-Goetze failure envelopes for a thermotectonic age of 500 Ma. Other parameters are as in (B) except that a strong, dry, Maryland diabase has been assumed for the lower crust. The two envelopes show other possible rheological models: in one, the upper and lower crusts are strong and the mantle is weak (upper panel); in the other, the upper and lower crusts and the mantle are strong (lower panel). The assumption of a strong lower crust in the weak mantle model again contributes little to  $T_e$  because of decoupling, although  $T_e$  would increase from 20 to 40 km if the upper crust was strong at its interface with the lower crust. In contrast, a strong lower crust contributes significantly to the  $T_e$  of the strong mantle model. This is because the lower crust is strong at its interface with the mantle and so the crust and mantle are mechanically coupled.

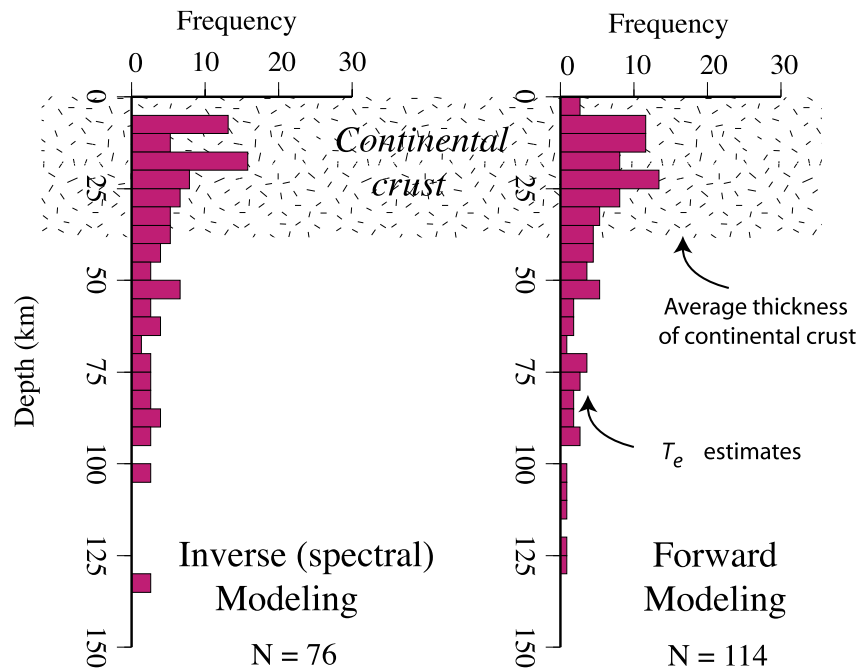
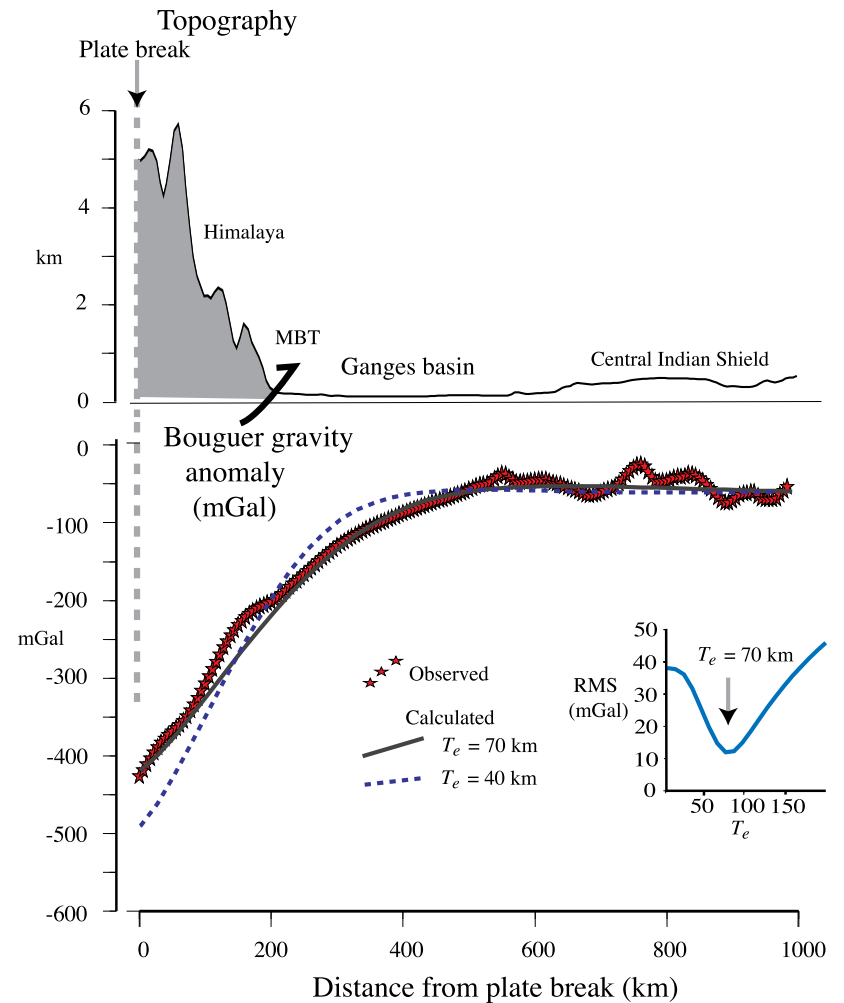


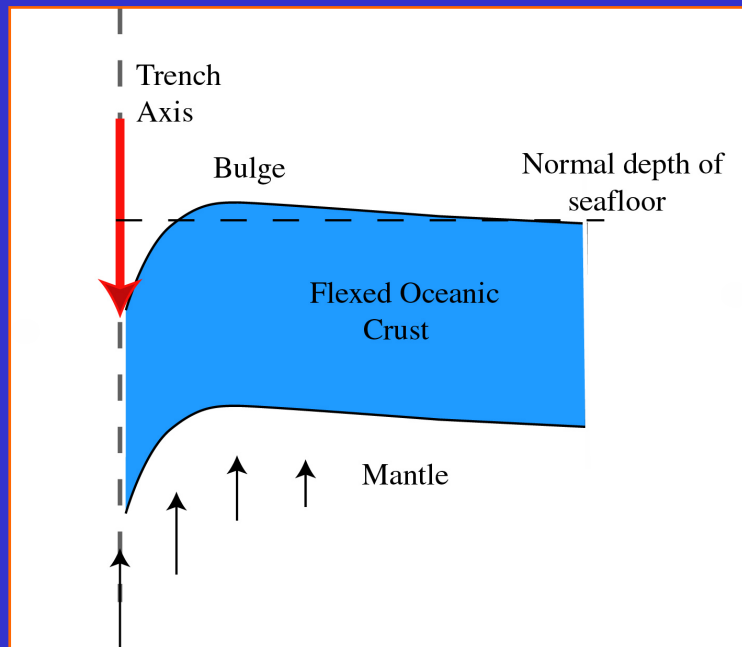
Figure 2. Histograms showing continental  $T_e$  estimates based on forward and inverse (i.e., spectral) gravity anomaly modeling methods. The histograms are based on data in Tables 5.2 and 6.2b of Watts (2001) and references therein. The data reflect a mix of tectonic settings. The spectral estimates mainly reflect old cratons, but include orogenic belts and rifts. The forward estimates are mainly from foreland basins. They reflect mainly rifts, since their mechanical properties are usually inherited during foreland basin formation, but include old cratons. The two modeling methods yield similar results and show that continental lithosphere is characterized by both low and high  $T_e$  values. In general, low values correlate with rifts, intermediate values with orogenic belts, and high values with old cratons. N—number of estimates.



# Topography seaward of the Kuril Trench

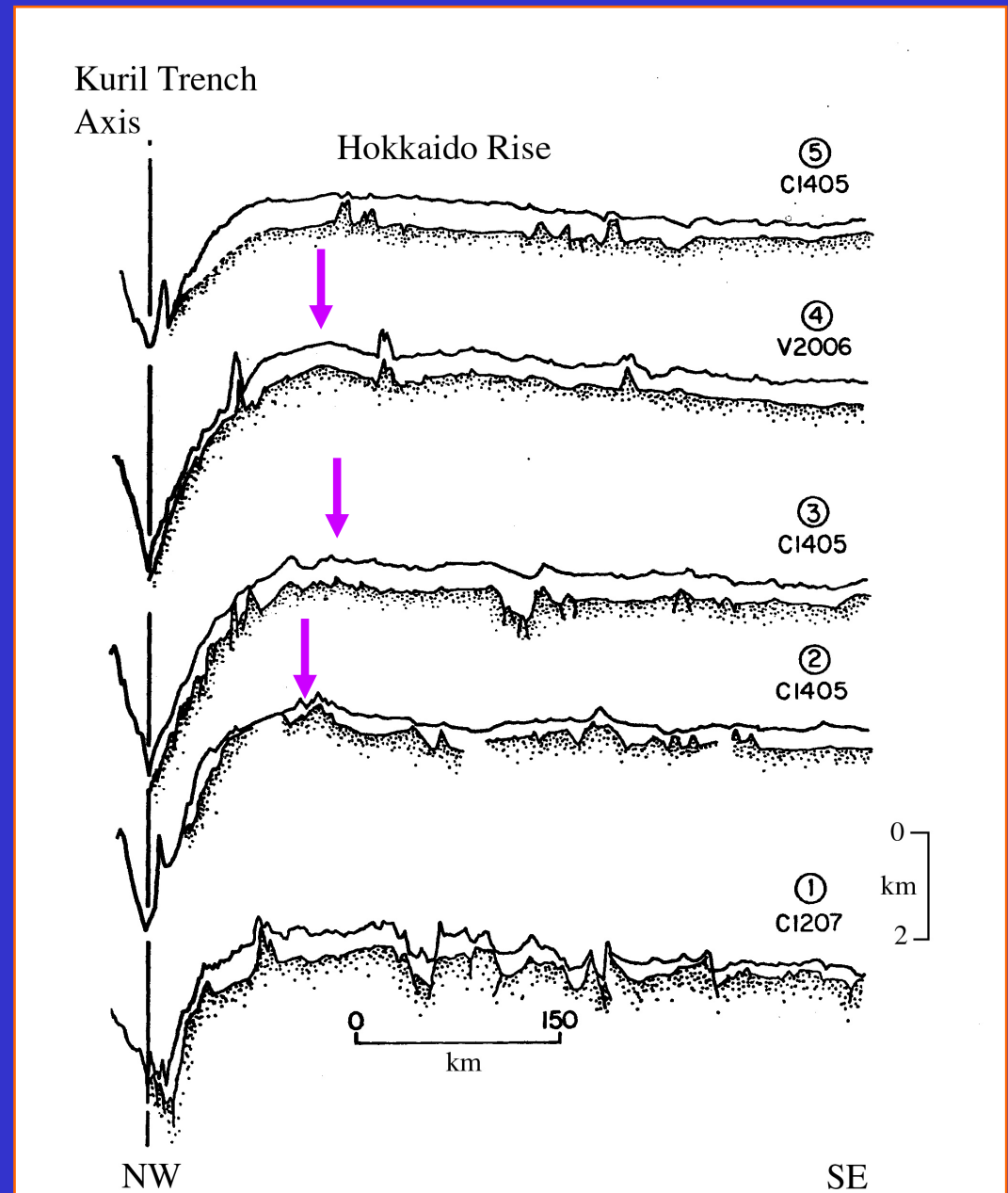
trench  
flexure:

plastic hinge  
zone

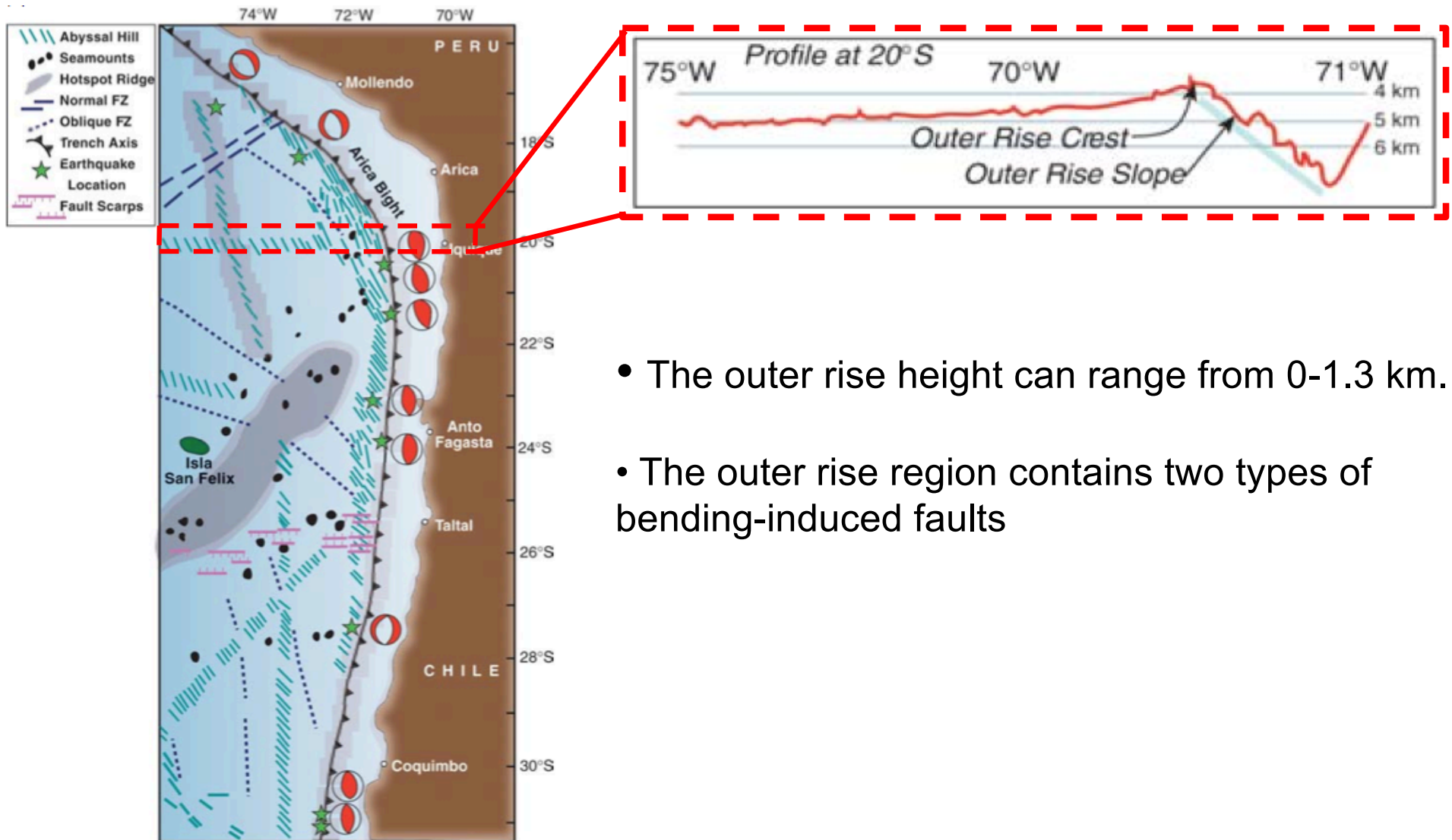


Distance to bulge  $\sim$  120-140 km

$T_e \sim$  30 km



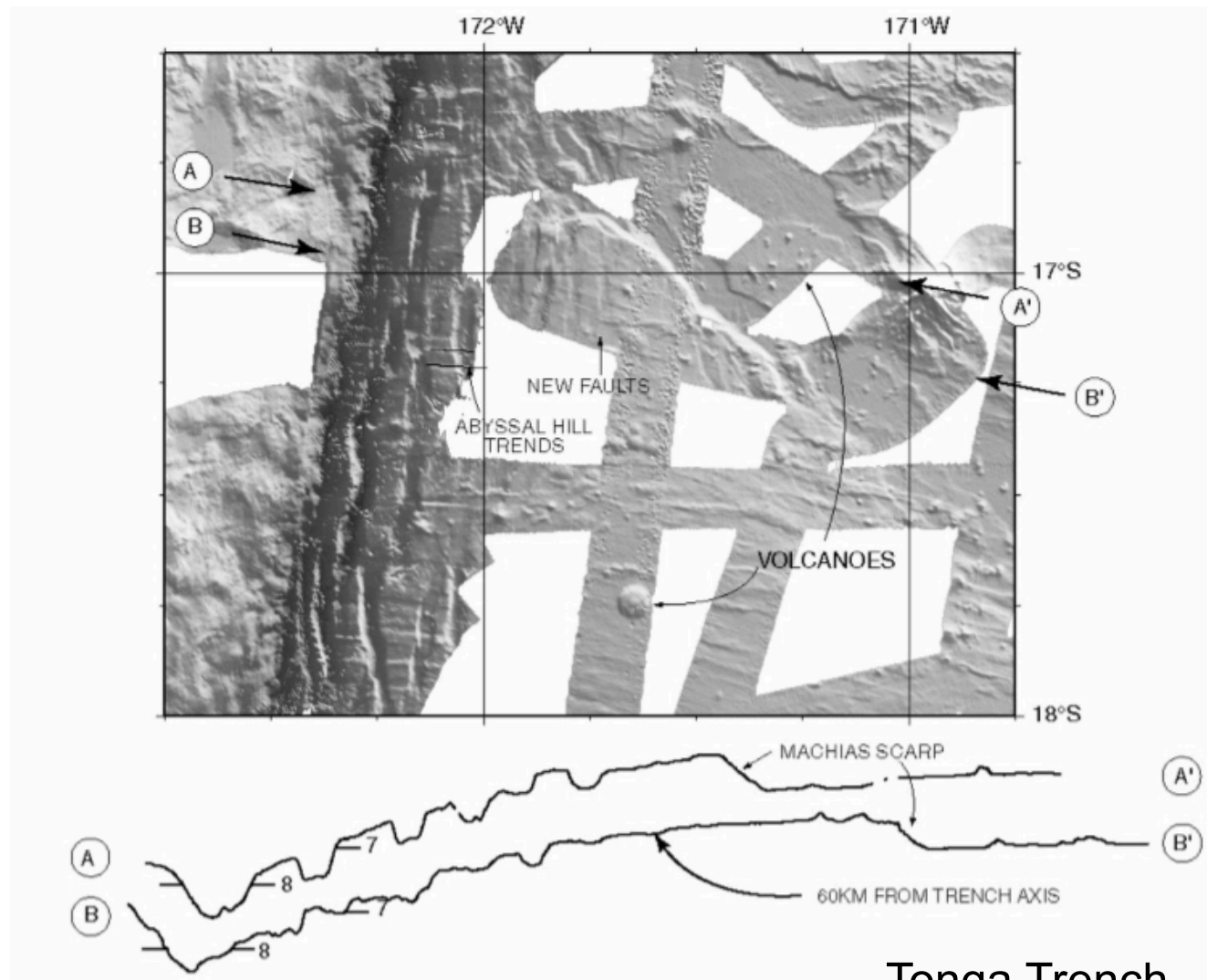
# outer trench wall fractures



- The outer rise height can range from 0-1.3 km.
- The outer rise region contains two types of bending-induced faults

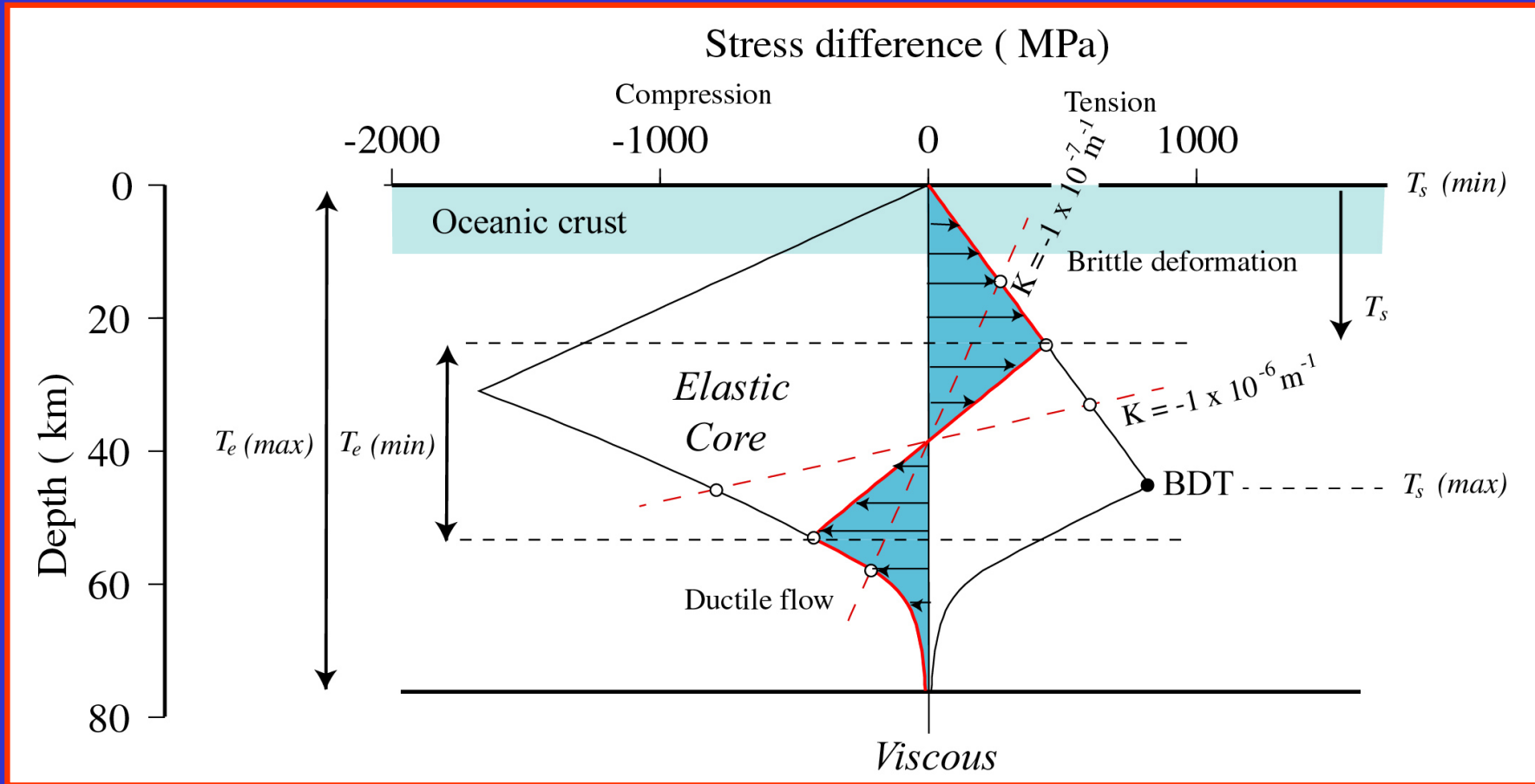
[Mofjeld et al., 2004]

# fractures



Tonga Trench  
[Massell – 2001]

# yield strength envelope



**Oceans** : earthquakes occur in the sub-oceanic mantle, but the mantle is also involved in the support of long-term loads.

**Continents** : earthquakes are rare in the sub-continental mantle, but it is still involved in the support of long-term loads

# Yield Strength Envelope

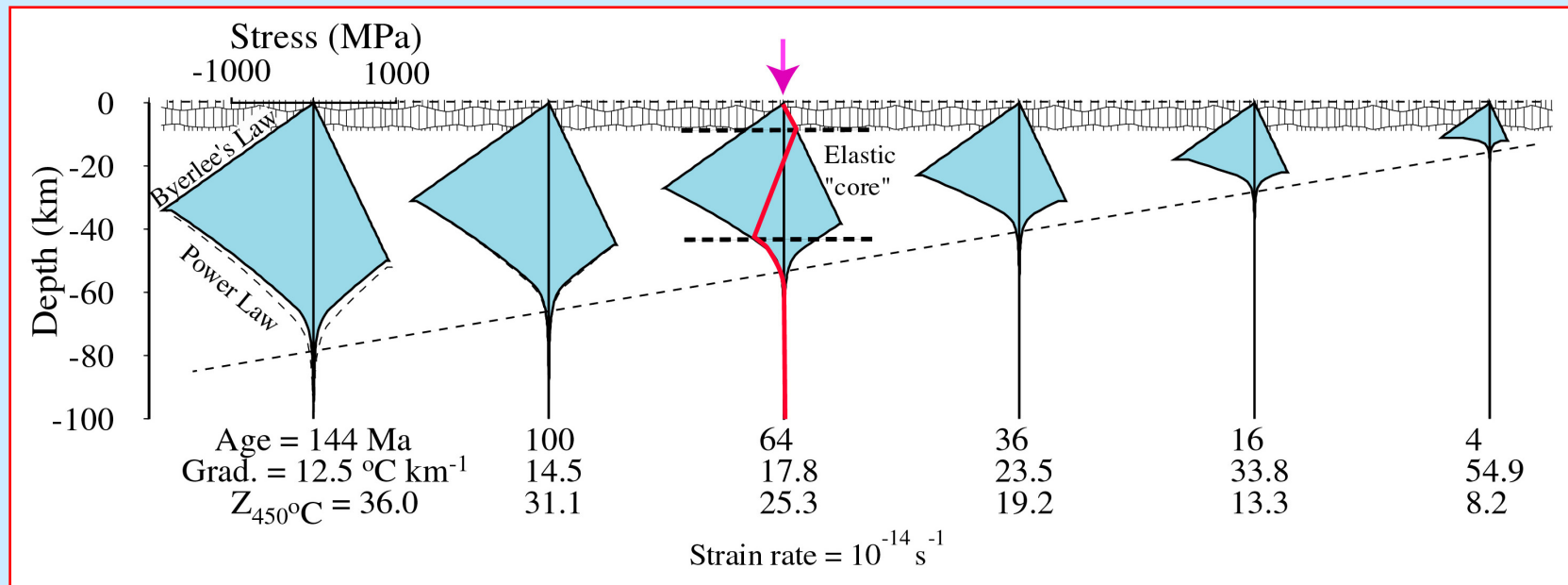
The Yield Strength Envelope (YSE) combines the **brittle** and **ductile** deformation laws of rock mechanics into a single strength profile for the lithosphere.

The ductile flow law is given by:

$$\dot{\epsilon} = A_p (\sigma_1 - \sigma_3)^n e^{-\frac{Q_p}{R_g T}}$$

where  $n$  is a positive integer,  $A_n$  is the power law stress constant,  $(\sigma_1 - \sigma_3)$  is the stress difference,  $Q_p$  is the power law activation energy,  $R_g$  is the universal gas constant and  $T$  is temperature.

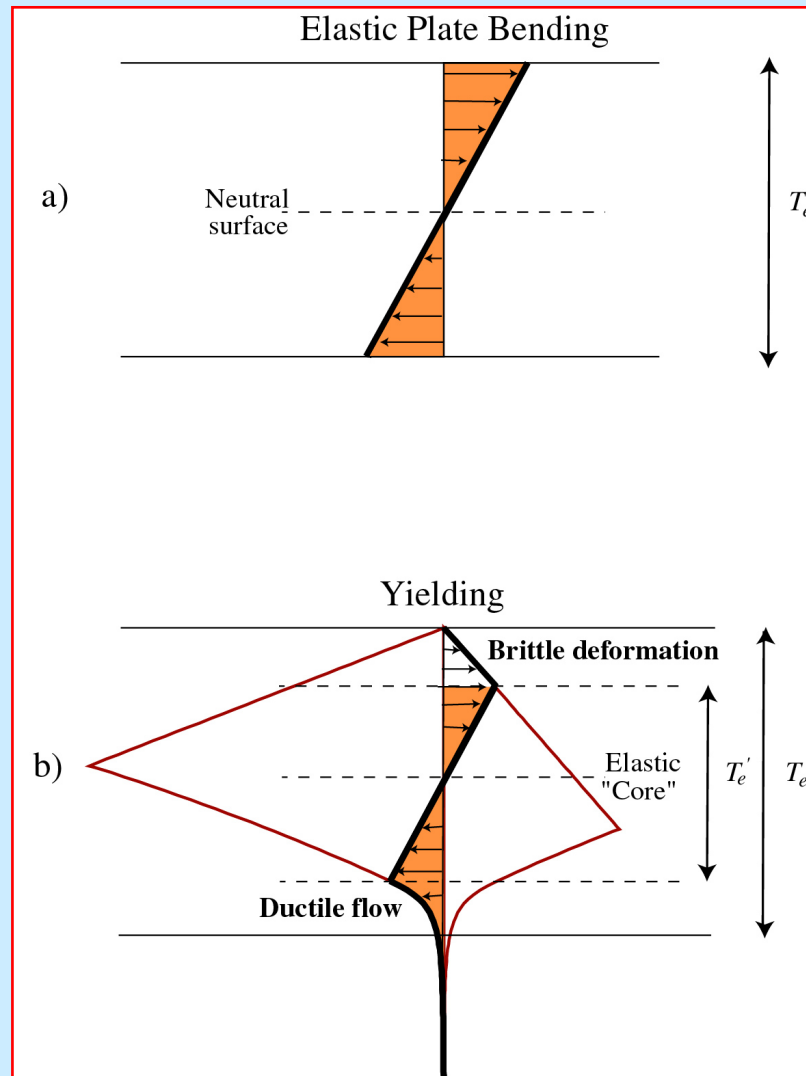
[Olivine :  $n=3$ ,  $A_n = 7.0 \times 10^{-14}$  and  $Q_p = 520 \text{ kJ mol}^{-1}$ ]



The area under the YSE is a measure of the **integrated strength** of the lithosphere. The YSE shows that the thickness of the strong zone is greater than the elastic core and increases linearly with the square root of age.

[slides provided by Tony Watts]

# $T_e$ and the Yield Strength Envelope



The elastic model implies that all stresses are supported elastically and that the maximum stresses accumulate in the uppermost and lowermost part of the plate.

$$M_{elastic} = \int_{\frac{T_e}{2}}^{-\frac{T_e}{2}} \sigma_x y_f dy$$

$$\frac{1}{r} = K = \frac{-M_{elastic} 12 (1 - \nu^2)}{E T_e^3}$$

In the YSE model, however, stresses are relieved by **brittle** failure in the uppermost part of the plate and by **ductile** flow in the lowermost part.

$$M_{YSE} = M_{upper} + M_{core} + M_{lower}$$

$T_e'$  of an inelastic plate (ie one that yields) can be computed from  $M_{YSE}$  by assuming it to have the same curvature as an elastic plate.